MITSUBISHI ELECTRIC RESEARCH LABORATORIES
https://www.merl.com

Motor Fault Detection with a Hybrid Physics-based and Data-Driven Method

Ji, Dai-Yan; Wang, Bingnan; Inoue, Hiroshi; Kanemaru, Makoto

TR2025-062 May 20, 2025

Abstract

Electric machine condition monitoring and fault detection using machine learning methods have been widely investigated in recent years. One main challenge for such data-driven approaches is the lack of real data, especially for machines under faulty conditions. In this paper, we propose a framework to address the data scarcity problem with a hybrid physics-based and data-driven method, and evaluate the effectiveness on induction motor eccentricity fault detection. We first use a simulation model to generate synthetic data for the motor under eccentricity fault; then we introduce a topological data analysis method to process the obtained data and extract fault-related features; next we apply domain adaptation technique to bridge the gap between the synthetic data and limited real data; finally with the adapted data, we train machine learning models to predict motor fault conditions. We show the prediction error is reduced from over 12% to about 5% compared with the same model trained without the domain adaptation process.

IEEE International Electric Machines and Drives Conference (IEMDC) 2025

Mitsubishi Electric Research Laboratories, Inc.
201 Broadway, Cambridge, Massachusetts 02139

Motor Fault Detection with a Hybrid Physics-based and Data-Driven Method

Dai-Yan Ji
Center for Industrial Artificial Intelligence,
University of Maryland,
College Park, MD 20742, USA

Bingnan Wang
Mitsubishi Electric Research Laboratories (MERL)
201 Broadway, Ste 8
Cambridge, MA 02139 USA

Hiroshi Inoue
Advanced Technology R&D Center
Mitsubishi Electric Corporation
Amagasaki, Hyogo 661-8661 Japan

Makoto Kanemaru
Advanced Technology R&D Center
Mitsubishi Electric Corporation
Amagasaki, Hyogo 661-8661 Japan

Abstract: Electric machine condition monitoring and fault detection using machine learning methods have been widely investigated in recent years. One main challenge for such data-driven approaches is the lack of real data, especially for machines under faulty conditions. In this paper, we propose a framework to address the data scarcity problem with a hybrid physics-based and data-driven method, and evaluate the effectiveness on induction motor eccentricity fault detection. We first use a simulation model to generate synthetic data for the motor under eccentricity fault; then we introduce a topological data analysis method to process the obtained data and extract fault-related features; next we apply domain adaptation technique to bridge the gap between the synthetic data and limited real data; finally with the adapted data, we train machine learning models to predict motor fault conditions. We show the prediction error is reduced from over 12% to about 5% compared with the same model trained without the domain adaptation process.

I. Introduction

Electric machines are widely used in a variety of industry applications and electrified transportation systems, and their condition monitoring and fault detection are important in protecting assets and avoiding safety hazards. Traditionally, motor fault detection replies on sensing modalities such as vibration and acoustic emission [1]. Motor current signature analysis (MCSA) approach, on the other hand, has a few promising advantages compared with other sensing methods, such as simple implementation and low cost [2]. MCSA detects motor faults based on the measured motor current data, and requires no additional sensor installation [3]. With the understanding of the physical mechanism of faults, MCSA conducts detailed signal analysis, and relates the specific frequency components in the stator current spectrum to each type of fault. One main challenge with MCSA is that the fault signals are often much smaller and dominated by the fundamental component and its harmonics. In addition, it is impossible to have a model to completely describe all the conditions in the physical motor system, and there are always discrepancies between physical models and real system. Therefore fault signals in real data can be different than those identified with physical model [4], and it is difficult to identify the fault signals in real data and determine the fault condition based only on physical models.

In recent years, the advancements of machine learning and deep learning techniques have attracted wide interest toward electric machine fault detection and condition monitoring [5]. Trained on experiment data, these learning-based models have the capability of extracting latent features in high-dimensional data related to the fault condition of the machine, and perform fault classification or regression tasks. However, for such data-driven approach to work with reasonable accuracy, sufficient measurement data are needed to train the models. In the case of electric machines, measurement data from faulty conditions are particularly difficult to obtain, as most data are collected when the machines are healthy. Another drawback for data-driven approaches is limited generalization capability. Models that are trained and work well on one particular dataset often do not work on new datasets that are not seen by the model before.

To address this challenge, we develop a fault detection method which combines physics-based and data-driven approaches to improve the fault detection performance as well as the generalization capability. We first utilize a simulation model to generate synthetic stator current data for an electric motor under fault conditions. We then perform topological data analysis on the time-domain data to better reveal fault-related features. While the model can reasonably simulate the fault condition, there are unavoidably discrepancies between synthetic and real data. In the next step, with the obtained synthetic data and some limited real measurement data, we develop domain adaptation (DA) technique [6] to bridge the gap between synthetic and real data. After simulation-to-real (Sim2Real, or S2R) DA, the synthetic data are more aligned

This work was done when D. Ji was with Mitsubishi Electric Research Laboratories as research intern. Corresponding Author: Bingnan Wang (bwang@merl.com).

with real data. With the synthetic data after S2R DA process, we train machine learning models to make predictions for the fault condition. After training process, the model is deployed for fault detection, where it takes in the real data, and make predictions for the fault condition of the machine.

The rest of the paper is organized as follows. In Section II we define the problem and describe the proposed framework and methodology for each step in the framework. In Section III, we introduce the data collection and processing process and analyze the obtained data. In Section IV, we introduce the numerical experiment settings to validate the effectiveness of proposed method on fault detection performance, present and discuss the results. Finally we conclude the paper in Section V.

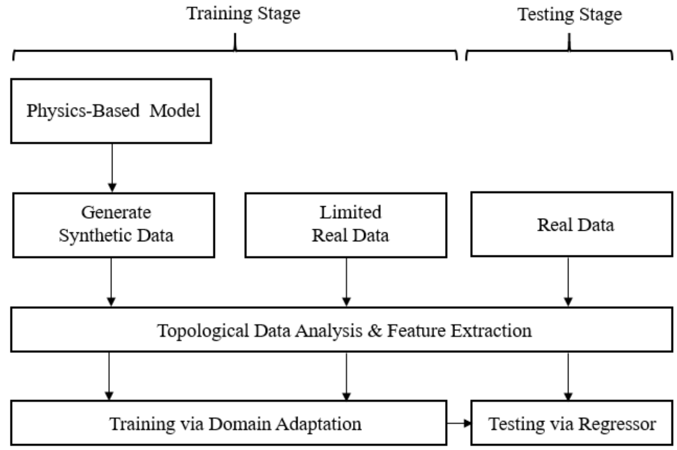

Fig. 1: A framework of the proposed methodology for motor eccentricity detection.

II. PROBLEM DEFINITION & METHODOLOGY

This study evaluates the effectiveness of the proposed method in detecting the level of eccentricity faults in an induction motor. Eccentricity occurs when the rotor and stator are not concentric, which is a common issue in motors and the main problem addressed in this study. An elevated eccentricity level causes stator winding faults and rubbing between stator and rotor. Monitoring the eccentricity condition during motor operation plays a crucial role in preventing machine failures and protecting assets. Detection of eccentricity can be achieved using MCSA by analyzing the spectrum of stator current, where certain components indicate the presence of the fault. However, the fault signatures in stator current can be very small and difficult to quantity, making it difficult to accurately identify the eccentricity level. To address the problem of detecting eccentricity faults in induction motors, we present a novel methodology, as illustrated in Fig. 1. The initial step involves generating synthetic data through a physics-based model (Section II-A). Subsequently, features are extracted using topological data analysis techniques (Section II-B). To bridge the gap between synthetic and real data, a domain adaptation (DA) strategy based on optimal transport is employed during the training stage (Section II-C), using synthetic data as the source domain and limited real data as the target domain. Finally, the trained model's performance is assessed on real data during the testing stage.

A. Physics-based Model

A physics-based model is developed for the purpose of generating synthetic data that accurately represent the diverse range of eccentricity conditions present within the experimental framework. The key parameters include motor design, supply voltage, load, and fault conditions, which determine the inductance terms between rotor and stator windings at each rotor position. These inductance terms, along with their derivatives, are computed using the Modified Winding Function Method (MWFM) [1], [7], [8], updating at each rotor position to capture the motor's dynamic behavior. The motor dynamics are then simulated through coupled circuit equations to obtain stator current signals. The inductance between winding i and winding j is expressed as:

$$L_{ij}(t) = \mu_0 l r \int_0^{2\pi} n_i(\phi,t) M_j(\phi,t) g^{-1}(\phi,t)\, d\phi. \quad (1)$$

Here, μ_0 represents the permeability of free space, while r and l denote the motor's air-gap radius and stack length, respectively. The terms $n_i(\phi,t)$ and $M_j(\phi,t)$ correspond to the winding function of coil i and the modified winding function of coil j, respectively.

The air gap function $g(\phi,t)$ is crucial in modeling motor performance under Static Eccentricity (SE) and Dynamic Eccentricity (DE) conditions:

$$g(\phi,t) = g_0 K_c - \delta_{\mathrm{SE}} g_0 \cos(\phi) - \delta_{\mathrm{DE}} g_0 \cos(\phi - \omega_r t), \quad (2)$$

where g_0 is the nominal air gap length, K_c is Carter's coefficient, and δ_{SE} and δ_{DE} represent the amplitudes of SE and DE, respectively. The detailed modeling process is described in [9]. While the simulation does not perfectly match experimental data due to inevitable model simplifications, it identifies key signal features attributable to eccentricity. The generated synthetic data provides valuable insights into motor faults by reflecting the non-uniform air gap distribution, crucial for accurate fault diagnosis and system analysis. In this study, we run simulations for the motor with SE level from 5% to 70%, with step size of 5%, and record the stator current data.

B. Topological Data Analysis & Feature Extraction

Topological Data Analysis (TDA) provides a numerical method to extract intrinsic shape information from data spaces. TDA has several advantages that make it highly attractive for data analysis: it is invariant under small and continuous deformations, coordinate-free, and robust to noise. Using these strengths, TDA can effectively process time-domain current data from different eccentricity conditions without preprocessing to distinguish subtle differences. The TDA method has been shown to be effective in extracting fault-related features and differentiating data from different eccentricity levels [10].

In this study, we summarize the overall procedure to calculate persistent homology, exhibit persistent diagram, adopt Betti curve as a representation, and extract ten statistical features as the following six steps:

1) A *point cloud* is established by collecting time-domain 3-phase current data. We generate this point cloud by segmenting the data and embedding it within a 3D Euclidean space. Different sampling and embedding techniques can be employed to optimize this process.
2) The *simplicial complex* of the point cloud is identified, essentially employing *Rips complex* [11], a prevalent algorithm in TDA. This approach constructs the simplicial complex by defining a threshold value or filtration radius r, and includes only those simplices where the pairwise Euclidean distances between data points do not exceed r. The simplicial complex comprises various topological building blocks, such as points, edges, and triangles, across multiple dimensions.
3) *Homology* H_i is computed from the constructed simplicial complex, where the subscript i indicates the dimension. Specifically, H_0 enumerates the number of connected components.
4) *Persistent homology* [12] is derived through a filtration process of the Rips complex. This process computes the homology at various filtration radius r, tracking each topological feature's "birth" (b) and "death" (d) at respective r. Persistent homology is represented in a persistence diagram consisting of points (b, d), where $b, d \in \mathbb{R}^2$ and $d > b$, each depicting the lifespan of a topological feature "born" at radius b and "dead" at radius d.
5) A *Betti curve* is derived from transforming a persistence diagram. We analyze the persistence diagram D, comprising a set of points $\alpha = (b_\alpha, d_\alpha)$, each representing the birth and death of topological features. We define a maximum filtration radius $r_{\max}$ and an array of equally spaced points $\{r_i\}_{i=1}^{M}$ within $[0, r_{\max}]$. The Betti sequence $\vec{\beta} = (\beta_i)_{i=1}^{M}$ is calculated by applying the function:

$$f_\alpha(r) = \begin{cases} 1, & \text{if } b_\alpha \leq r \leq d_\alpha, \\ 0, & \text{otherwise}, \end{cases} \tag{3}$$

At each r_i, the Betti number β_i is computed as:

$$\beta_i = \sum_{\alpha \in D} f_\alpha(r_i) \tag{4}$$

6) *Statistical features*, from the H_0 Betti Curve, provide a quantitative analysis derived from the zeroth homological dimensions of the data set across varying filtration radius. These features include ten primary statistical measures: area, slope, intercept, R-value, mean, standard deviation, interquartile range (IQR), skewness, kurtosis, and root mean square (RMS), detailed in Table I.

C. Domain Adaptation

While the synthetic data is reasonably good in modeling the eccentricity fault, there are unavoidable differences between the synthetic and real data. In this step, we try to bridge the gap between the synthetic data obtained from simulations and the real data from experiment measurements using domain adaptation (DA). DA aims to reduce the distributional discrepancy between the source domain D_s and the target domain D_t by mapping their feature distributions. In our case, the source domain D_s contains synthetic data with varying SE levels, ranging from 5% to 70%, while the target domain D_t consists of real data with only two SE levels: 7.1% and 57.3%. Feature vectors, denoted as X_s and X_t, are generated by extracting features from the source and target domains, respectively. These vectors are subsequently used in the domain adaptation process, where they are aligned.

Many DA techniques have been developed to address different types of problems. In this paper, we formulate DA as a regularized optimal transport (OT) problem [13]. By adding an entropy term to the traditional transport cost function, the purpose is to achieve improved computational efficiency and solution smoothness:

$$\gamma^* = \arg\min_{\gamma} \sum_{i,j} \gamma_{i,j} C(x_s^i, x_t^j) + \epsilon \sum_{i,j} \gamma_{i,j} \log(\gamma_{i,j}) \tag{5}$$

where the transport plan is denoted by γ, the function $C(x_s^i, x_t^j)$ defines the penalty for moving mass from location x_s^i in the source distribution to location x_t^j in the target distribution, and the regularization parameter, ϵ, controls the trade-off between minimizing the transport cost and maximizing the entropy of the transport plan. The cost matrix C represents the pairwise distances between source and target domain data points, commonly calculated using the squared Euclidean distance: $C_{i,j} = \|x_s^i - x_t^j\|^2$.

Due to the computational expense of solving the entropy-regularized Optimal Transport problem, the Sinkhorn algorithm is adopted to efficiently approximate the transport plan γ while ensuring numerical stability. Given the cost matrix C and a regularization parameter ϵ, the Sinkhorn kernel K is defined as: $K = \exp\left(-\frac{C}{\epsilon}\right)$. The Sinkhorn algorithm updates the dual variables u and v, which serve as scaling factors for the source and target distributions. The updates proceed iteratively:

$$u^{(k+1)} = \frac{\mathbf{r}}{K v^{(k)}}, \quad v^{(k+1)} = \frac{\mathbf{c}}{K^T u^{(k+1)}} \tag{6}$$

where $\mathbf{r}$ and $\mathbf{c}$ are normalized distribution vectors ensuring the marginal constraints of the optimal transport formulation. This iterative process continues until convergence, yielding the final transport plan:

$$\gamma^* = \text{diag}(u) K \text{diag}(v) \tag{7}$$

The computed transport plan γ^* is then used to transform the source domain data into the target domain space: $X_s^{trans} = \gamma^* X_s$. This transformation ensures the source data distribution matches the target domain. After the DA process, a regression model is trained using the transported source domain data

Table I: Statistical Features Extracted from H_0 Betti Curve

No.	Feature Name	Feature Description
1	Area $= \int \beta(r)\,dr$	Area under the curve calculated using trapezoidal integration
2	Slope $= \frac{\Delta y}{\Delta x}$	Slope of the linear regression line fitted to the curve
3	Intercept $= b$ from $y = mx + b$	Intercept of the linear regression line fitted to the curve
4	$R =$ correlation coefficient	R-value from the linear regression indicating the strength of correlation
5	$\mu = \frac{1}{n}\sum_{i=1}^{n}\beta_i$	Mean value of the Betti numbers over the filtration range
6	$\sigma = \sqrt{\frac{1}{n}\sum_{i=1}^{n}(\beta_i - \mu)^2}$	Standard deviation of the Betti numbers, measuring dispersion
7	IQR $= Q_3 - Q_1$	Interquartile range (IQR), representing the middle 50% of the Betti numbers
8	Skewness $= \frac{\sum_{i=1}^{n}(\beta_i-\mu)^3}{n\sigma^3}$	Skewness of the Betti numbers, indicating the asymmetry of the data distribution
9	Kurtosis $= \frac{\sum_{i=1}^{n}(\beta_i-\mu)^4}{n\sigma^4}$	Kurtosis of the Betti numbers, measuring the tails' heaviness
10	RMS $= \sqrt{\frac{1}{n}\sum_{i=1}^{n}\beta_i^2}$	Root mean square (RMS) of the Betti numbers, indicating the magnitude of data

$\{X_s^{trans}, Y_s\}$. The training model is tested with real data only to evaluate the performance

III. Data Analysis

While the synthetic data for this work are generated by the physical model described in Section II, real data for the domain adaptation study are recorded from an experimental setup.

A three-phase, 0.75 kW, 2-pole-pair squirrel-cage induction motor was modified for the experiment [10], [14], [15] to enable controlled levels of SE, as shown in Fig. 2. The motor has 36 stator slots, 28 rotor bars, a nominal air gap of 0.28 mm, operates at 200 V line-to-line voltage, and runs at 60 Hz. To facilitate precise adjustments, the original bearings were replaced, and the rotor is supported by two custom mounting structures with new bearings on the extended rotor shaft (with only the load-side structure visible in the figure). The stator assembly is mounted on a linear stage, allowing horizontal adjustments via micrometers. Additionally, displacement sensors positioned on the stator monitor real-time air gap variations in both horizontal and vertical directions during operation A powder brake is coupled to the motor to serve as a load.

In our experiment, data were collected from three-phase current sensors and four air gap sensors at a sampling frequency of 10 kHz for each SE condition under no-load operation. Six SE levels were set in the horizontal direction while the motor remained stationary, corresponding to air gap deviations of 7.1%, 16.5%, 31.1%, 42.5%, 47.5%, and 57.3% relative to the nominal air gap size. The air gap sensor measurements across all cases confirmed that the actual SE levels closely matched the initial settings, with deviations remaining within 3%, while also indicating a minor DE of approximately 6%.

The same data processing step using topological data analysis is performed for both synthetic and real data. More specifically, to analyze signal characteristics, we extract 1,024 consecutive data points from the stator current in time-domain, corresponding to approximately 0.1 seconds of measurement data at a 10 kHz sampling rate. Fig. 3 (a) presents synthetic data at an SE level of 30%, while Fig. 3 (b) shows real data at 31.1%, both recorded under no-load conditions. The corresponding H_0 Betti curves for all SE levels are shown in Fig. 3 (c) and Fig. 3 (d) for synthetic and real data, respectively. Compared with time-domain signals, the Betti curves allow us to distinguish data from different fault conditions more easily. Although the line shapes of synthetic and real data do not match exactly, the curves exhibit the same trend with increasing eccentricity.

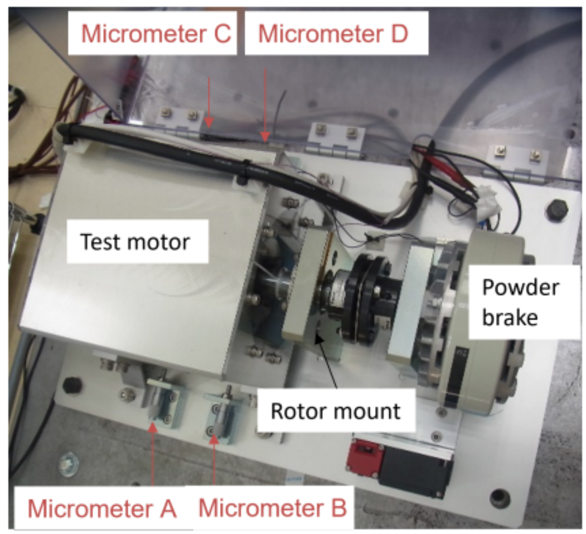

Fig. 2: The experimental configuration for analyzing induction motor eccentricity.

In the next step, we will address the differences between the synthetic and real data, and bridge the gap using domain adaptation. Instead of applying the H_0 Betti curves directly for domain adaptation, we further reduce the dimensionality of the data by extracting ten statistical features from the obtained Betti curves, and feeding the extracted features for domain adaptation. The list of features extracted from the H_0 Betti curves is shown in Table I.

Table II: Experiment Design and Test Results

Data	Real Data (Baseline)	Synthetic Data without Domain Adaptation	Synthetic Data with Domain Adaptation
Training	Real Data (7.1, 57.3 levels)	All Synthetic Data	All Synthetic Data + Real Data (7.1, 57.3 levels)
Testing	Real Data (16.5, 31.1, 42.5, 47.5 levels)		
Test RMSE (%)	12.16	23.31	5.47
Test MAE (%)	11.32	22.93	4.83

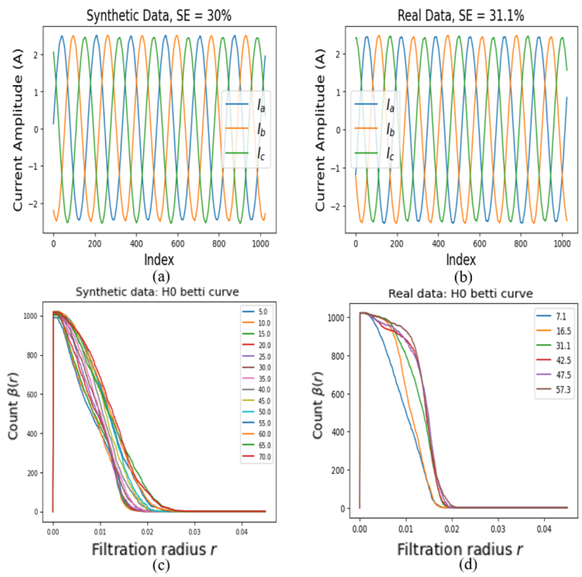

Fig. 3: Synthetic data (a) at SE level of 30% and real data (b) at SE level of 31.1%. H_0 Betti curves for synthetic data (c) across all SE levels and real data (d).

IV. Experiment Design & Results

With features extracted from the processed data, we apply domain adaptation to bridge the gap between synthetic and real data. To validate the effectiveness of the proposed method, we design three different numerical experiments, which are summarized in Table II:

1) Real Data (Baseline): Due to practical constraints, real data collection is limited to extreme SE levels (7.1% and 57.3%) for training, while data from intermediate SE levels (16.5%, 31.1%, 42.5%, and 47.5%) serve as the testing set.
2) Synthetic Data without DA: A physics-based model generates synthetic data (SE levels: 5%–70%, in 5% intervals) for training, with the testing set identical to that of the baseline experiment.
3) Synthetic Data with DA: DA is applied to synthetic data (at SE levels: 5%–70%), incorporating real data (at SE levels: 7.1% and 57.3%), with the same testing set as the previous two experiments.

The training set includes 7,350 synthetic samples (525 samples at each SE level) and 100 real samples (50 samples for each SE level at 7.1% and 57.3%, reflecting real-world data scarcity). The testing set includes 4,680 real samples (1,170 samples per SE level), each representing a 0.1-second measurement at 10 kHz sample rate. The same data pre-processing and feature extraction process shown in Section II-B is performed for all data samples. Domain adaptation is performed according to the optimal transport method shown in Section II-C. After that, we train a regression model to make predictions to the eccentricity level. A regression model using support vector regression with a radial basis function kernel (SVR-RBF) is built and trained with the proposed methodology. Models are trained to minimize the root-mean-squared-error (RMSE) and mean-absolute-error (MAE) on the SE level prediction.

The test results are also shown in Table II. As we can see, with model trained with synthetic data only, the RMSE is highest at 23.3%; with model trained with real data only at SE level 7.1% and 57.3%, the RMSE is 12.16%. This shows that there are discrepancies between synthetic data and real data, and we cannot solely reply on synthetic data from physical model. On the other hand, model trained with only limited real data is difficult to predict unseen new data. With our proposed DA strategy, the training data is enriched by combining synthetic data with limited real data, and the model performance is much improved, with RMSE reduced to around 5%. Fig. 4 provides a visual distribution of SE level predictions. These violin plots allow us to observe the spread and concentration of prediction values based on the experiment design.

To better understand the effect of domain adaptation, we present the t-distributed stochastic neighbor embedding (t-SNE) plot for data samples after TDA processing and feature extraction in Figure 5. Using statistical features extracted from H_0 Betti curve, Fig. 5 (a) illustrates that without DA, the distributions of source and target data are not well-aligned. However, as shown in Fig. 5 (b), applying DA with the OT method significantly improves alignment, bringing the adapted source data distribution closer to that of the target data.

These results demonstrate the effectiveness of the proposed method in enhancing data and improving the performance of machine learning based fault detection, using synthetic data generated by a physics-based simulation model, and domain adaptation. The proposed framework is flexible and can be easily applied to many other fault detection tasks. A variety of signal processing techniques, feature extraction methods,

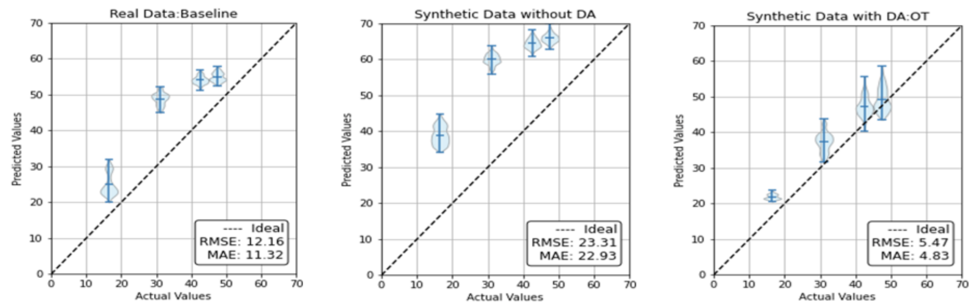

(a) (b) (c)

Fig. 4: Violin plot of SE level predictions on test data under to compare (a) real data: baseline, (b) synthetic data without DA, and (c) synthetic data with DA using OT.

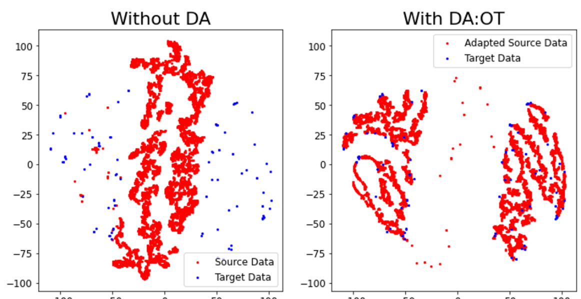

(a) (b)

Fig. 5: t-SNE plot in 2d for features extracted from H_0 betti curve at: (a) Without DA and (b) With DA.

domain adaptation methods, and machine learning models can be used to replace those presented in this work.

V. Conclusions

This study presents a groundbreaking approach to motor fault detection by integrating physics-based modeling with data-driven techniques. By applying topological data analysis to extract statistical features from both synthetic and real data, and subsequently aligning these domains through simulation-to-real adaptation, the results show a marked improvement in predictive performance, yielding more precise and robust fault detection. This innovative framework offers substantial improvements in fault detection accuracy and generalization capabilities, making it particularly valuable in scenarios where extensive real fault data is difficult to obtain. Future work can further refine this methodology to address more complex fault detection scenarios in electric machines.

References

[1] S. Nandi, S. Ahmed, and H. A. Toliyat, "Detection of rotor slot and other eccentricity related harmonics in a three phase induction motor with different rotor cages," *IEEE Transactions on Energy Conversion*, vol. 16, no. 3, pp. 253–260, 2001.

[2] J. Faiz and B. M. Ebrahimi, "Static eccentricity fault diagnosis in an accelerating no-load three-phase saturated squirrel-cage induction motor," *Progress in electromagnetics research*, vol. 10, pp. 35–54, 2008.

[3] K. N. Gyftakis and J. C. Kappatou, "A novel and effective method of static eccentricity diagnosis in three-phase psh induction motors," *IEEE Transactions on Energy Conversion*, vol. 28, no. 2, pp. 405–412, 2013.

[4] J. Faiz, B. M. Ebrahimi, B. Akin, and H. A. Toliyat, "Comprehensive eccentricity fault diagnosis in induction motors using finite element method," *IEEE Transactions on Magnetics*, vol. 45, no. 3, pp. 1764–1767, 2009.

[5] S. Zhang, S. Zhang, B. Wang, and T. G. Habetler, "Deep learning algorithms for bearing fault diagnostics—a comprehensive review," *IEEE Access*, vol. 8, pp. 29 857–29 881, 2020.

[6] A. Farahani, S. Voghoei, K. Rasheed, and H. R. Arabnia, "A brief review of domain adaptation," *Advances in data science and information engineering: proceedings from ICDATA 2020 and IKE 2020*, pp. 877–894, 2021.

[7] N. A. Al-Nuaim and H. Toliyat, "A novel method for modeling dynamic air-gap eccentricity in synchronous machines based on modified winding function theory," *IEEE Transactions on energy conversion*, vol. 13, no. 2, pp. 156–162, 1998.

[8] L. Zhou, B. Wang, C. Lin, H. Inoue, and M. Miyoshi, "Static eccentricity fault detection for psh-type induction motors considering high-order air gap permeance harmonics," in *2021 IEEE International Electric Machines & Drives Conference (IEMDC)*. IEEE, 2021, pp. 1–7.

[9] B. Wang, M. W. Albader, H. Inoue, and M. Kanemaru, "Induction motor eccentricity fault analysis and quantification with modified winding function based model," in *2022 25th International Conference on Electrical Machines and Systems (ICEMS)*. IEEE, 2022, pp. 1–6.

[10] B. Wang, C. Lin, H. Inoue, and M. Kanemaru, "Induction motor eccentricity fault detection and quantification using topological data analysis," *IEEE Access*, vol. 12, pp. 37 891–37 902, 2024.

[11] C. Tralie, N. Saul, and R. Bar-On, "Ripser. py: A lean persistent homology library for python," *Journal of Open Source Software*, vol. 3, no. 29, p. 925, 2018.

[12] G. Carlsson, "Topology and data," *Bulletin of the American Mathematical Society*, vol. 46, no. 2, pp. 255–308, 2009.

[13] N. Courty, R. Flamary, D. Tuia, and A. Rakotomamonjy, "Optimal transport for domain adaptation," *IEEE transactions on pattern analysis and machine intelligence*, vol. 39, no. 9, pp. 1853–1865, 2016.

[14] B. Wang, C. Lin, H. Inoue, and M. Kanemaru, "Topological data analysis for electric motor eccentricity fault detection," in *IECON 2022 – 48th Annual Conference of the IEEE Industrial Electronics Society*, 2022, pp. 1–6.

[15] B. Wang, H. Inoue, and M. Kanemaru, "Motor eccentricity fault detection: Physics-based and data-driven approaches," in *2023 IEEE 14th International Symposium on Diagnostics for Electrical Machines, Power Electronics and Drives (SDEMPED)*. IEEE, 2023, pp. 42–48.